AGU PUBLICATIONS

JGR

Journal of Geophysical Research: Atmospheres

RESEARCH ARTICLE

10.1002/2015JD024475

The temporal evolution of a long-lived contrail cirrus cluster: Simulations with a global climate model

Lisa Bock[1] and Ulrike Burkhardt[1]

[1]Deutsches Zentrum für Luft- und Raumfahrt, Institut für Physik der Atmosphäre, Oberpfaffenhofen, Germany

Key Points:
- Contrail cirrus with two-moment microphysics as independent cloud class in a climate model
- Microphysical processes control the lifetime of contrail cirrus in long-lived ice supersaturated areas
- In aged contrail cirrus deposition is limited due to low ice crystal number concentration

Correspondence to:
L. Bock,
lisa.bock@dlr.de

Citation:
Bock, L., and U. Burkhardt (2016), The temporal evolution of a long-lived contrail cirrus cluster: Simulations with a global climate model, *J. Geophys. Res. Atmos.*, *121*, 3548–3565, doi:10.1002/2015JD024475.

Received 11 NOV 2015
Accepted 4 MAR 2016
Accepted article online 10 MAR 2016
Published online 14 APR 2016

Abstract The representation of contrail cirrus in climate models has advanced in the last years tremendously. Nevertheless, uncertainties in particular regarding the representation of contrail microphysics still remain. Properties of young contrail cirrus differ from those of natural cirrus due to the large ice crystal number concentration common in contrails. Consequently, microphysical process rates in contrail cirrus, which control its lifetime, can be very different to those in natural cirrus. We extend a contrail cirrus scheme within a climate model by implementing a microphysical two-moment scheme and study the life cycle of a contrail cirrus cluster. In an idealized experiment we study the properties and microphysical process rates of a contrail cirrus cluster in a large and long-lived ice supersaturated region. We find that at flight level contrail cirrus display their typical high ice crystal number concentration (of about 10–100 cm^{-3}) for a few hours with far lower densities in lower levels caused by sedimentation. After about 7 h contrail cirrus have spread considerably so that even at flight level associated ice crystal number concentrations have dropped to values that prohibit fast relaxation of ice supersaturation. The reduced ice crystal number and the resulting limited water uptake in the contrail cirrus limit the lifetime of the contrail cirrus cluster to about 10 h even though surrounding conditions would be still favorable for contrail cirrus persistence. In our case studies, contrail cirrus resembles natural cirrus regarding their ice crystal number concentration and size after 5–7 h.

1. Introduction

Aviation contributes 3–8% to the overall anthropogenic forcing [*Lee et al.*, 2009]. Of the aviation effects the radiative forcing due to contrail cirrus, consisting of linear contrails and the cirrus clouds arising from them, is larger than that due to CO_2 accumulated from aviation [*Burkhardt and Kärcher*, 2011; *Boucher et al.*, 2013]. With a projected yearly growth of the aviation sector of about 5% [*ICAO*, 2007] the climate effect of contrail cirrus is growing in importance.

Contrails form in air that is cold and moist enough so that an aircraft plume reaches water saturation when mixing with the surrounding air [*Schumann*, 1996] and can persist as long as air is at least ice saturated. Scattering of shortwave radiation by ice crystals leads to a reduction of solar radiation at the Earth surface, which has a cooling effect. On the other hand absorption and emission of longwave radiation reduce the terrestrial outgoing radiation, because absorbed infrared radiation is emitted at significantly lower temperatures than from the Earth surface. This warming effect dominates on average for optically thin ice clouds such as contrail cirrus [*Meerkötter et al.*, 1999].

The contrail cirrus climate impact is determined by contrail cirrus microphysical properties and coverage. Important factors controlling contrail cirrus microphysical properties are the total number of ice crystals formed [*Kärcher et al.*, 2015] and surviving the vortex phase [*Unterstrasser*, 2014; *Lewellen*, 2014] and the amount of water vapor deposited on ice crystals. The latter is, in particular in the beginning of the contrail lifetime, dependent on relative humidity and on the growth of the contrail cirrus volume. The evolution of the ice crystal number concentration is determined by the number of ice crystals surviving the vortex phase, the air volume mixed into the contrail and by microphysical process rates and can limit the overall amount of water that can be deposited on ice crystals. Deposition is dependent on the level of ambient moisture available for deposition and on the ice crystal concentration and controls the growth of ice crystals and therefore sedimentation rates. Contrail cirrus volume is not only mainly controlled by the interaction of shear and sedimentation [*Lewellen*, 2014] but also by turbulent diffusion [*Dürbeck and Gerz*, 1996]. Microphysical properties and process rates in contrail cirrus depend strongly on the age of the contrail. In young contrails many

small ice particles compete for the water vapor available for deposition. Within the contrail cirrus core area ice supersaturation is reduced efficiently by deposition on the ice crystals [*Heymsfield et al.*, 1998] which leads to ice particle growth. The evidence of ice crystal sedimentation can sometimes, in highly ice supersaturated air, be seen in large fall streaks [*Atlas et al.*, 2006]. Microphysical and optical properties of aged contrail cirrus change and are thought to eventually resemble those of neighboring cirrus.

The evolution of single contrails and their detailed microphysical development is successfully simulated using large eddy simulations (LES) models [e.g., *Jensen et al.*, 1998; *Lewellen*, 2014; *Paoli et al.*, 2013; *Paoli and Shariff*, 2016; *Unterstrasser and Gierens*, 2010]. The very high temporal and spatial resolution and detailed microphysical parameterizations allow a realistic simulation of the development of young contrails. Later on, the contrail life cycle is often dominated by changes in the synoptic situation and contrails may interact or overlap with other contrails or natural clouds. In order to resolve this interaction, contrail cirrus development is studied in models resolving the evolution of the atmospheric state, e.g., in numerical weather prediction or climate models. Within those models the representation of contrails is naturally coarser; nevertheless, if the climate impact of contrails is to be estimated in a climate model, the main properties of contrail cirrus development need to be captured despite the low resolution. Here we show that our contrail parameterization is able to simulate those main properties and their evolution.

Representing contrail cirrus in climate models, many simplifications are usually made. Contrails may be simply treated as a source term for the ice crystal budget of the natural cirrus, mixing the microphysical properties of natural ice clouds and contrails [*Chen et al.*, 2012], and making resulting changes in ice cloud properties difficult to interpret. Given the nonlinear nature of microphysical processes this mixing can introduce biases in the microphysical process rates of both natural clouds and contrail cirrus. Contrail cirrus evolution may be calculated offline without feedback on the moisture or energy budget of the atmosphere and with limited knowledge of cloud vertical overlaps [*Schumann*, 2012], which are crucial for estimating radiative fluxes. While representing contrail cirrus within a climate model as an independent cloud class the contrail cirrus scheme of *Burkhardt and Kärcher* [2009] captures the competition between contrail cirrus and natural cirrus for available water vapor. The decrease of natural cirrus as feedback process is included. Nevertheless, the parameterization relies on a one-moment microphysical scheme treating microphysical processes as a function of ice water content only. This means that microphysical and optical differences and the resulting differences in microphysical process rates between contrail cirrus and natural cirrus (or old and young contrail cirrus) that are caused by differences in particle number concentrations could not be represented. The dependence of water vapor deposition on ice crystal number concentrations could not be resolved neglecting the fact that aged contrail cirrus may have very low ice crystal number concentrations that may not allow the relaxation of supersaturation within a model time step.

In this paper we aim at studying the evolution of a contrail cirrus cluster in a large scale and long-lived ice supersaturated area. This kind of situation is particularly suited to the evaluation of the microphysical scheme of the contrail cirrus parameterization due to two reasons: First, the evolution of contrail cirrus and the role of microphysical process rates limiting the lifetime of the cluster can be analyzed. Second, long-lived contrail cirrus clusters have a large impact on contrail cirrus cover and on contrail cirrus radiative forcing. Therefore, their representation in a model should be examined. We develop an improved contrail cirrus parameterization based on the work of *Burkhardt and Kärcher* [2009] using a microphysical two-moment scheme based on the work of *Lohmann et al.* [2008]. In section 2.1 we describe the changes to the natural cloud scheme which were necessary in order to make the fractional cloud cover of *Sundqvist* [1978] consistent with the two-moment microphysics of *Lohmann et al.* [2008] in the ice cloud regime, a prerequisite for simulating contrail cirrus. In section 2.2 we introduce the new contrail cirrus parameterization. We discuss how the life cycle of contrails, including their microphysical development, can be described in a general circulation model (ECHAM5-CCMod) and which processes need to be captured to resolve microphysical properties realistically. In particular the representation of water vapor deposition, that is limited for young contrails by the contrail volume and for aging contrail cirrus by the ice crystal number density, turned out to be important. The parameterization of the increase in contrail cirrus volume is based on turbulent diffusional growth and the interplay of vertical wind shear and sedimentation (Appendix A). In section 2.3 we introduce an idealized experiment and discuss the evolution and the microphysical process rates of the contrail cirrus cluster (section 3). We study the contrail cirrus life cycle in a long-lived and large-scale ice supersaturated synoptic situation since microphysical process rates have a maximum impact on the contrail cirrus life cycle in those situations. We compare the ice crystal dilution seen on average within the contrail cirrus cluster with LES estimates

(section 3.1) and discuss the impact of dilution on supersaturation relaxation (section 3.2) and the limitation of water uptake due to low ice crystal number concentrations within old contrail cirrus or in areas that are dominated by sedimenting ice crystals. We analyze how fast contrail cirrus microphysical and optical properties (section 3.3) resemble those of natural cirrus. The microphysical evolution of the idealized study is compared with two more long-lived contrail cirrus clusters in section 3.4. Conclusions are summarized in section 4.

2. Model and Data

2.1. The Natural Cloud Scheme

We base our model development on the ECHAM5-HAM model [*Roeckner et al.*, 2003; *Stier et al.*, 2005] including the microphysical two-moment scheme of *Lohmann et al.* [2008]. The latter introduces grid mean ice supersaturation consistent with the microphysics of ice clouds. Since the fractional cloud cover scheme [*Sundqvist*, 1978] is unable to deal with ice supersaturation, the introduction of grid mean ice supersaturation results in an all or nothing cloud cover in the ice cloud regime. Fractional cloud cover is crucially important in low resolution models and is a prerequisite for simulating contrail cirrus. We reintroduce fractional cloud cover, b_{ci}, as a function of relative humidity, r [*Sundqvist*, 1978], also for the ice cloud regime:

$$b_{ci} = 1 - \sqrt{1 - \frac{r - r_{ci}}{r_{\mathrm{sat}} - r_{ci}}}. \tag{1}$$

When r exceeds the critical relative humidity for natural cloud formation, r_{ci}, cloud coverage is larger than zero. r_{ci} is resolution dependent. In our simulations $r_{ci} = 0.7$. Full cloud coverage is realized, when relative humidity reaches saturation, $r_{\mathrm{sat}} = 1$. We assume that in a newly formed cloud, a cloud that was not transported into the grid box, the homogeneous nucleation threshold is reached. In this case ice nucleation is triggered in the fraction of the grid box occupied by the new cloud while the grid box is grid mean subsaturated. This gives us the possibility of keeping changes to the natural cloud microphysics scheme at a minimum while regaining fractional cloud cover. In adapting the natural cloud scheme we make a trade-off. *Lohmann et al.* [2008] resolve the nucleation events at grid mean ice supersaturation while degrading the cloud cover scheme, whereas we reintroduce the fractional cloud cover also for ice clouds while having to make assumptions about triggering of nucleation events. In order to simulate both fractional cloud cover and ice supersaturation leading to nucleation events consistently, it would be necessary to introduce a fully prognostic cloud scheme [*Kärcher and Burkhardt*, 2008].

Ice nucleation is triggered distinguishing between already existing cirrus and newly developed cirrus. We assume that a positive increment of cirrus cover, calculated from the diagnostic cloud cover parameterization, relative to the preexisting advected cirrus cover represents newly developed cirrus, whereas the remaining cirrus cover is assumed to be old. We estimate the nucleation of ice crystals, considering only homogeneous nucleation, in the following way: (1) In a newly developed cloud, relative humidity is assumed to have reached the nucleation threshold. Following *Kärcher and Lohmann* [2002] the number of nucleated ice crystals is calculated dependent on the nucleation threshold relative humidity, the vertical velocity, which is approximated in our model by the resolved vertical velocity and its subgrid variability, estimated from the turbulent kinetic energy (TKE), as in the original microphysical two-moment scheme [*Lohmann and Kärcher*, 2002]. (2) Within an existing cloud secondary nucleation is allowed and calculated in the same way as the primary ice nucleation in the newly clouded area except that the cooling rate, that drives the nucleation event, is decreased due to the deposition on existing ice crystals [*Kärcher et al.*, 2006]. (3) Finally in case the cloud cover parameterization indicates that a cirrus has newly formed and the cooling rate is very small or even negative (less than 0.1 mm/s) we estimate the nucleated ice crystal number in the following way. Assuming an average temperature-dependent ice crystal radius [*Wang and Sassen*, 2002] we infer the nucleated ice crystal number from the deposited water (resulting from saturation adjustment within the cloud). This is an uncommon situation and associated ice crystal nucleation rates have a small impact on the overall nucleation rate. They are on average at least one and in many areas several orders of magnitude smaller than the nucleation rate described under 1 and 2. (4) If cirrus cover decreases we keep ice crystal number density constant. Note that the largest uncertainty estimating ice nucleation comes from the uncertainty in the subgrid variability of the vertical wind velocity which is driving the nucleation event. Comparing to aircraft data, it has been shown that using the TKE approach, the representation of the vertical wind variability and the associated nucleation events are

largely improved as compared to using only resolved vertical winds [*Kärcher and Ström*, 2003]. *Hoyle et al.* [2005] use a probability density function of subgrid-scale variability of the cooling rate derived from aircraft measurements and show that following a trajectory in the European Centre for Medium-Range Weather Forecasts model the imposed subgrid-scale variability greatly improves their simulated ice crystal number densities, whereas the TKE approach gives slightly smaller number concentrations. Nevertheless, large uncertainties remain.

Water vapor deposition is calculated driving in-cloud relative humidity down to saturation within a time step. We do not allow ice supersaturation within the cloud.

After introducing the above modifications to the cloud scheme, we retuned the model to be in radiative equilibrium. We stay within the parameter range explored by *Lohmann and Ferrachat* [2010] except for the parameters dealing with the autoconversion rate and the entrainment rate for deep convection, which we set to values slightly lower/higher than Lohmann and Ferrachat to be 0.5 and $2.5 \cdot 10^{-4}$, respectively. We perform a 10 year simulation in T42L41 with a time step of 15 min and predescribed Atmospheric Model Intercomparison Project II sea surface temperatures. This model configuration with 41 vertical layers (16 above 200 hPa and 25 below) is used because of the increased vertical resolution, about 500 m, near the tropopause [*Kurz*, 2007]. Since we introduced changes only to the in situ formed and therefore mostly thin ice clouds we use the CFMIP Observation Simulator Package (COSP) satellite simulator [*Bodas-Salcedo et al.*, 2011; *Nam and Quaas*, 2012] in order to compare the simulated cloud cover above 440 hPa to observations from Calipso [*Chepfer et al.*, 2010]. The satellite simulator calculates from model data the ice cloud coverage that a satellite instrument could have detected enabling a fair comparison with satellite observations. The comparison indicates that our cloud cover is slightly overestimated by up to 10% (Figure 1a). This overestimation mainly results from a generally too large cloud cover in the subtropics and an overestimation outside the midlatitude storm tracks. Both problems may be due to the low resolution in our model (T42L41). The common model bias (cold bias) in polar regions with a too high tropopause contributes to an overestimation of polar cloud cover.

The dependence of the simulated ice water content on temperature (Figure 1b) matches closely results from aircrafts measurements [*Schiller et al.*, 2008] taking into account the uncertainty in this dependence. For the comparison model data are sampled similarly to aircraft measurements in three regions: Arctic (January–March from 58 to 75°N in 5 – 13 km height), midlatitudes (October–December from 40 to 70°N in 6 – 14 km height), and tropics (January, February, March, November, and December from −23 to 23°N in 8.5 – 19 km height). The model may be overestimating IWC at low temperatures. This bias likely results from a relatively high ice water content in the tropical upper troposphere in the simulations [*Nam and Quaas*, 2012; *Gehlot and Quaas*, 2012]. The simulated zonal mean grid mean ice crystal number concentration of natural clouds (Figure 2a) reaches maxima of 0.5 to 1 cm^{-3} at lower levels and of 0.1 cm^{-3} at temperatures below about 233 K. In our simulations ice crystals at lower model levels are mainly formed by freezing of cloud droplets.

Comparing with aircraft data collected in the months between January and June in an area between 85°W and 109°W and 26°N and 42°N (an area influenced strongly by convective activity) at heights between 6.5 and 15 km [*Jensen et al.*, 2013] our scheme agrees very well with observations at low temperatures (190–215 K). The probability of in-cloud ice crystal number concentrations is maximum at low number concentrations and the drop off in probability is near the value of 1 cm^{-3}. In the warmer regimes the probability of high (low) ice crystal concentrations is too high (low) in our model simulations (Figure 2b) relative to measurements. This mismatch between model simulations and measurements in this convectively active region is most likely resulting from an overestimation of the convective input and problems simulating its processing within the anvil. Convective events have a long-lasting impact on the amount of condensate and associated ice crystal number concentrations in the upper troposphere. But eventually, in aged anvil cirrus ice crystal number concentrations are typically not very different from those in cirrus formed in situ, e.g., *Jensen et al.* [2009]. The high frequency of large in-cloud ice crystal number concentrations may therefore be connected with both, difficulties in estimating the convective input in ice crystal number and in simulating the temporal evolution of the convective anvil. As the influence of convection on the ice crystal number concentration decreases with height and homogeneous nucleation becomes the dominant source of ice crystals at lower temperatures (190–215 K), the model appears to estimate ice crystal number concentrations of in situ formed cirrus realistically. *Jensen et al.* [2013] show that the measurements can be reproduced in detailed simulations with high resolution considering homogeneous nucleation only. This means that it is not likely that treating only

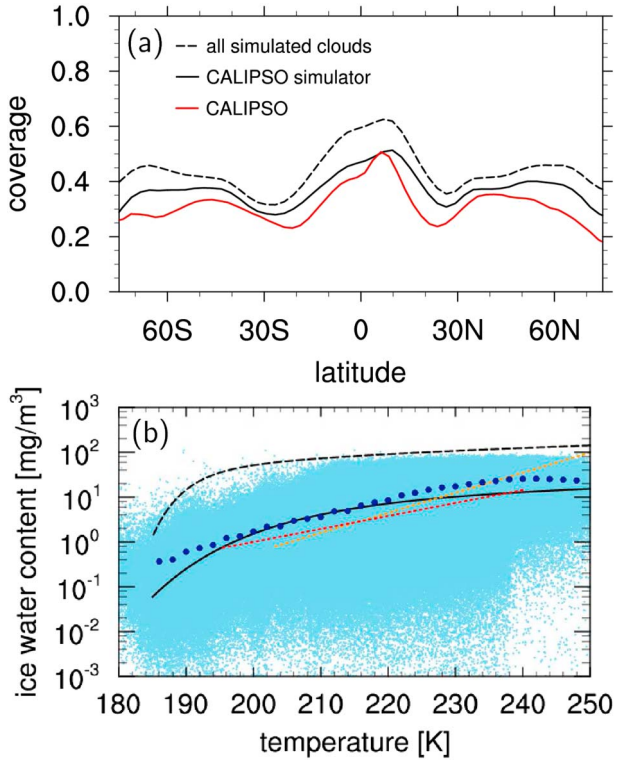

Figure 1. (a) Zonal mean cloud cover above 440 hPa of natural clouds as simulated by ECHAM5-CCMod (black dashed line) and when using the COSP satellite simulator (black solid line) in comparison to CALIPSO measurements (red line). (b) In-cloud ice water content variability as a function of temperature of natural clouds as simulated by ECHAM5-CCMod. The variability in modeled IWC is indicated by light blue dots and mean values (within 2 K bins) by fat dark blue dots. Black curves describe the mean (solid) and maximum values (99% envelop) (dashed) of IWC fitted to in situ observations from measurement campaigns [*Schiller et al.*, 2008]. Additionally, the mean IWC from other fits to in situ observations from the literature are shown: thin orange dotted line [*Schumann*, 2002] and red dotted line [*Wang and Sassen*, 2002; *Kärcher and Voigt*, 2006].

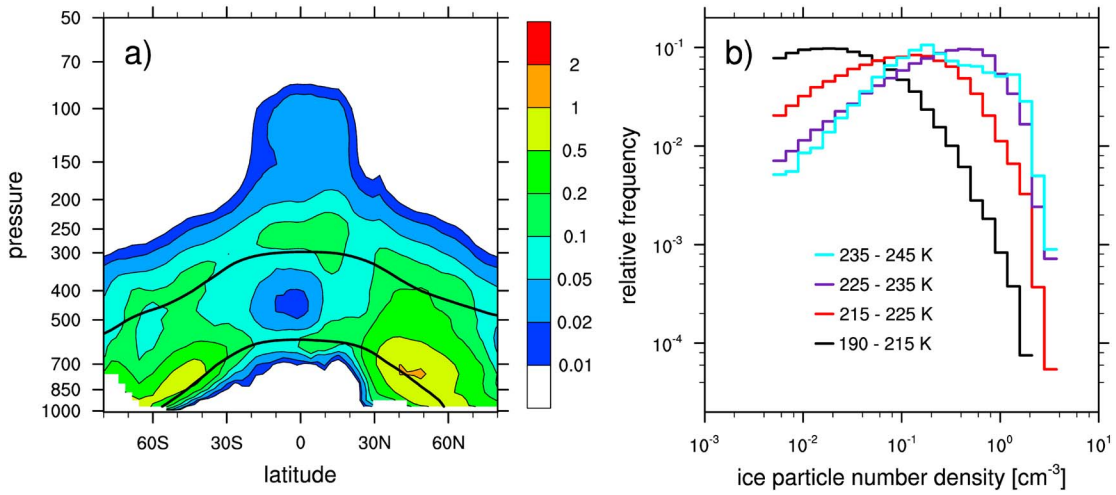

Figure 2. (a) Zonal mean grid mean ice crystal number concentration of natural clouds in [cm^{-3}] and (b) relative frequency of in-cloud ice crystal number concentrations of natural clouds for different temperature regimes as simulated by ECHAM5-CCMod. In Figure 2a the data are averaged over the whole grid box and is sampled over clear and cloudy periods, the solid black lines indicate 273 K and 235 K isolines. The probability of ice crystal number concentrations in Figure 2b is calculated from simulated values in the same geographical area and season as the aircraft measurements of *Jensen et al.* [2013]. As in the measurements the lower limit for ice crystal number concentrations was set to be 5 per liter.

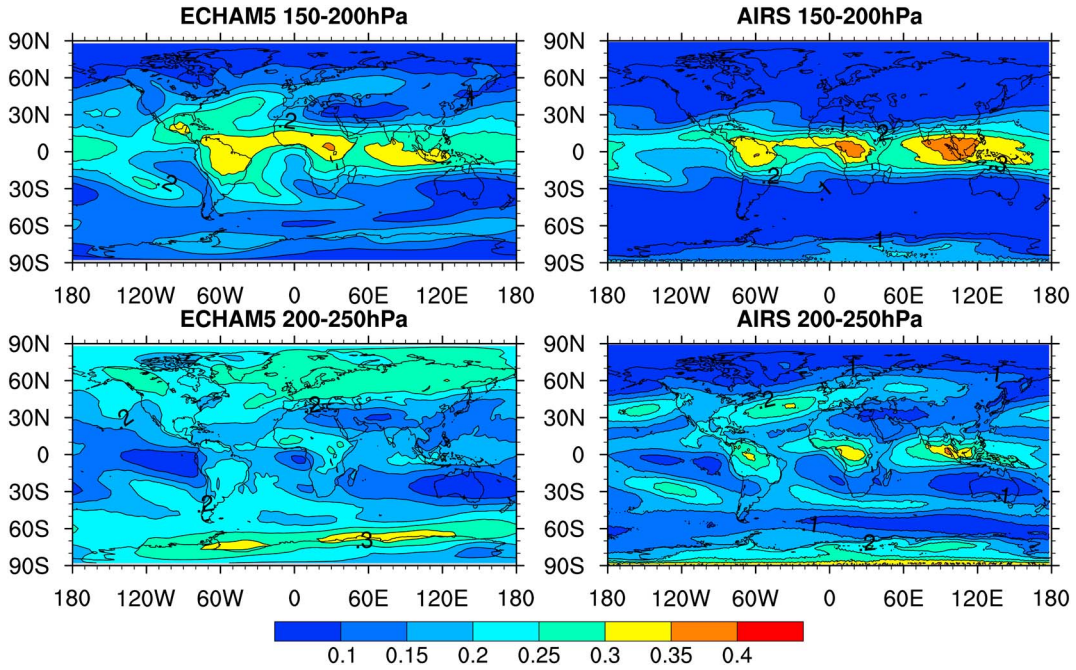

Figure 3. Frequency of ice supersaturation (left) in ECHAM5-CCMod and (right) in scaled AIRS satellite measurements [*Lamquin et al.*, 2012] in the upper troposphere.

homogenous ice nucleation in our model is the reason for the overestimation of the probability of high ice crystal number concentrations.

The fractional ice supersaturated area was parameterized according to *Burkhardt et al.* [2008] based on the information of subgrid variability of total water inherent in the cloud scheme. In Figure 3 the resulting ice supersaturation frequency is compared to Atmospheric Infrared Sounder (AIRS) satellite observations that were scaled using Measurement of OZone on Airbus In-service airCraft (MOZAIC) in situ measurements [*Lamquin et al.*, 2012]. Between 150 hPa and 200 hPa ice supersaturation frequency is well simulated with maxima in the tropics and low frequencies in the extra tropics. Simulated tropical maxima are slightly too low and are extending too far into the subtropics and extratropics indicating a too high tropopause in the latter areas. Ice supersaturation frequency between 200 hPa and 250 hPa is estimated successfully equatorward of about 50° latitude with slight underestimation of supersaturation frequency around the Intertropical Convergence Zone and in the areas of the storm tracks. Poleward of 50° the supersaturation frequency is significantly overestimated consistent with the too high tropopause. In those areas ice supersaturation frequency is underestimated in the level below (not shown) indicating that the maxima in upper tropospheric ice supersaturation are simply shifted upward relative to AIRS observations.

2.2. A Two-Moment Microphysical Scheme for Contrail Cirrus

The contrail cirrus scheme of *Burkhardt and Kärcher* [2009] forms the basis of our development. In this parameterization contrail cirrus are introduced as a new cloud class consistent with the natural cloud scheme. Rather than tracing and simulating individual contrails this scheme simulates the bulk contrail coverage and ice water content. Contrails form according to the Schmidt-Appleman criteria [*Schumann*, 1996] and evolve in ice supersaturated regions [*Burkhardt et al.*, 2008]. Contrail cirrus coverage increases due to vertical wind shear and water vapor deposition in contrail cirrus is dependent on the available water vapor. Prognostic variables are grid mean contrail cirrus cover and length, separated in age classes until the age of 5 h, and ice water content averaged over all contrail cirrus within the grid box. Contrail cirrus can affect the water budget and compete with natural clouds for available water vapor.

Consistent with the natural cirrus scheme in ECHAM5-HAM [*Lohmann et al.*, 2008] and our modifications (section 2.1), we extend the parameterization of contrail cirrus to a two-moment microphysical scheme,

with contrail cirrus ice crystal number concentration as a new prognostic variable. The conservation equation of the contrail cirrus variables is given by

$$\frac{\partial X}{\partial t} = \left(\frac{\partial X}{\partial t}\right)_{\text{tsp}} + \left(\frac{\partial X}{\partial t}\right)_{\text{sed}} + \left(\frac{\partial X}{\partial t}\right)_{\text{prc}} + \left(\frac{\partial X}{\partial t}\right)_{\text{spr}} + \left(\frac{\partial X}{\partial t}\right)_{\text{dif}} + \left(\frac{\partial X}{\partial t}\right)_{\text{dep/sub}} + \left(\frac{\partial X}{\partial t}\right)_{\text{new}}, \tag{2}$$

where X stands for contrail cirrus coverage (b), volume (V) and length (L), ice water content (q), and ice crystal number concentration (n). Many contrail cirrus processes, such as transport due to advection and vertical diffusion (tsp), sedimentation (sed), and precipitation (prc), have been parameterized in the same way as in the natural cloud scheme [*Roeckner et al.*, 2003]. Within the microphysical two-moment scheme the size dependency of microphysical processes, such as sedimentation, is described so that they adapt automatically to the smaller ice crystal sizes of young contrails. Contrail formation (new) and spreading due to vertical wind shear (spr) have been parameterized as in the contrail cirrus parameterization of *Burkhardt and Kärcher* [2009]. The parameterization of deposition/sublimation (dep/sub) has been adapted to be consistent with the cloud cover scheme while retaining the dependency on ice crystal number and sizes (see below). A parameterization of the increase in contrail cirrus volume due to turbulent diffusion (dif) has been added (Appendix A). The new, transport, sedimentation terms are relevant for all contrail cirrus variables; the spreading term is only relevant for the contrail cover; the volume increase due to turbulent diffusion has an impact on the contrail cirrus volume and in-cloud ice crystal number concentration; the deposition term changes only the IWC, and the precipitation term impacts only the ice water content and ice crystal number concentration. Note that besides adding new variables, contrail cirrus volume, and ice crystal number concentration, the parameterization of deposition and sedimentation is improved relative to the parameterization of *Burkhardt and Kärcher* [2009] due to the introduction of the two-moment microphysical scheme. As in the old scheme contrail cirrus are treated as an independent cloud class and microphysical processes are calculated for both cloud classes independently.

We initialize contrails at 7.5 min of age (half the model time step) after the vortex phase of the contrail. We set the initial ice crystal number concentration ($\left(\frac{\partial n}{\partial t}\right)_{\text{new}}$, equation (2)) to 150 particles cm^{-3}, an average value derived from measurements of contrails with an age of a few minutes [*Schumann*, 2002; *Febvre et al.*, 2009; *Schröder et al.*, 2000; *Voigt et al.*, 2011]. This ice crystal number concentration, at 7.5 min after contrail formation, corresponds to an apparent ice crystal number emission index of 4.5 to $5.5 \cdot 10^{14}$ per kg fuel. At formation, contrail cirrus were initialized with a contrail area cross section of 200 × 200 m and the flight distance that forms a contrail, as in *Burkhardt and Kärcher* [2009], giving an initial contrail volume per grid box ($\left(\frac{\partial V}{\partial t}\right)_{\text{new}}$, equation (2)). We estimate the development of contrail cirrus volume (Appendix A) which limits the water vapor deposition in young contrails. As the ice crystal number concentration decreases, deposition is reduced and the contrail cirrus cluster eventually ceases to exist. Except for limiting the deposition rate for young contrails, the contrail cirrus volume is of little significance for the physical processes describing the evolution of contrail cirrus.

2.2.1. Deposition

A good representation of deposition ($\left(\frac{\partial q}{\partial t}\right)_{\text{dep/sub}}$, equation (2)) is crucial since deposition determines the ice crystal growth and associated microphysical process rates. The grid mean available water vapor, Δq_v, is determined by the mass mixing ratio of water vapor, q_v, and the saturation mixing ratio over ice, q_{sat}:

$$\Delta q_v = q_v - q_{sat}. \tag{3}$$

Within young contrails Δq_v is equal to the deposition rate due to the typically very large ice crystal number concentrations [*Heymsfield et al.*, 1998; *Kärcher et al.*, 2015]. In the later contrail cirrus life stages, and in particular in areas dominated by sedimentation, this may not be the case. Instead, water vapor deposition may be controlled by the ice crystal number concentration and crystal size due to long diffusional growth time scales. Following *Korolev and Mazin* [2003] the available water vapor relaxes exponentially to saturation due to the presence of ice crystals

$$\frac{\partial \Delta q_v}{\partial t} = -\frac{\Delta q_v}{\tau}. \tag{4}$$

We estimate the time scale, τ, with which ice supersaturation can be relaxed due to diffusional growth in the following way:

$$\tau^{-1} = 4\pi \cdot D \cdot \Phi \cdot C \cdot r \cdot n \tag{5}$$

with the diffusion coefficient, D [*Pruppacher and Klett*, 1996], the ventilation factor, Φ [*Lohmann and Kärcher*, 2002], dependent on the sedimentation velocity, and the capacity of the ice particles, C, dependent on the ice particle form. (C is here assumed to be 1.1.) τ is dependent on the mass-weighted mean ice crystal size, r, and number density n. It increases with contrail cirrus lifetime due to the strong dilution and due to sedimentation and the resulting strong reduction in ice crystal number concentration.

We calculate the mixing ratio of deposited water per time step, Δq_{dep}, dependent on the temporal evolution of Δq_v:

$$\Delta q_{\mathrm{dep}} = \Delta q_v|_{\Delta t=0} - \Delta q_v|_{\Delta t} = \Delta q_v|_{\Delta t=0} \cdot (1 - e^{-\frac{\Delta t}{\tau}}). \tag{6}$$

In case of $\Delta t \gg \tau$ or $\Delta t \ll \tau$ the deposited water is equal $(\Delta q_v)|_{\Delta t=0}$ and 0, respectively. We approximate Δq_{dep} assuming that all available water is deposited if the model time step length, Δt, is much larger than the depositional time scale, τ. This is particularly the case at the beginning of the contrail cirrus life cycle. As soon as the time scale τ is larger than the model time step, we correct deposition with the correction factor $\frac{\Delta t}{\tau}$. Late in the life cycle or in the areas dominated by sedimentation Δt is significantly smaller than τ and the approximation is very good. When Δt is close to τ, e.g., at flight level after a few hours of lifetime (see section 3.2) we somewhat overestimate deposition.

We define a corrected volume, V_{corr}, which is the part of the contrail cirrus volume in which saturation is reached. The corrected volume is a measure for the part of the available water vapor in the total contrail cirrus volume, V, that is deposited on the contrail cirrus ice crystals and affects therefore the contrail cirrus ice water content. The change in contrail cirrus grid mean ice water content is calculated as follows:

$$\left(\frac{\partial q}{\partial t}\right)_{\mathrm{dep}} = \frac{V_{\mathrm{corr}}}{V_{\mathrm{gb}}} \cdot \Delta q_v = \frac{\Delta t}{\tau} \cdot \frac{V}{V_{\mathrm{gb}}} \cdot \Delta q_v \,, \tag{7}$$

with V_{gb} the total grid box volume. The fraction of the available water vapor that can be deposited on the ice crystals is proportional to the ice crystal number density and the ice particle size (equation (5)). The limitation of water deposition due to low ice crystal number concentrations is one of the most important improvements relative to the contrail cirrus parameterization of *Burkhardt and Kärcher* [2009] as it limits the optical depth of old and very diluted contrail cirrus.

2.3. Idealized Experiment

We perform an idealized simulation of a single contrail cluster and study its properties and temporal evolution. The air traffic density (distance per grid box) and water vapor emissions were prescribed using the AERO2k air traffic inventory [*Eyers et al.*, 2004]. Air traffic was switched on for 1 h over the eastern part of the U.S.A., southwest of the Great Lakes (34–44°N, 87–116°W) at 260 hPa in January. Therefore, the age of the simulated contrail cirrus in the cluster varies by up to 1 h only, allowing us to study the temporal evolution of contrail cirrus properties. The general circulation model (GCM) was run in T42L41 resolution. In the experiment region this translates into a geometric dimension of the Gaussian grid box of about 300 km × 200 km × 500 m (latitude × longitude × height). If one aircraft flies 30 km through this box and everywhere contrails would form, the contrail would fill 0.04% of the grid box volume at an age of 7.5 min. Assuming a wind shear of 0.006 s^{-1}, comparable to the situation in the idealized experiment, and considering only dilution and everywhere ice supersaturation, the contrail would fill about 1% of the grid box volume after 150 min.

We selected a synoptic situation which is characterized by a large-scale and long-lasting ice supersaturated area in winter. Contrails form in a large scale and long-lived ice supersaturated area ahead of a trough situated southwest of the Great Lakes at 260 hPa and between −55 to −60°C. In this area contrails coexist with natural cirrus and the large scale rising and cooling ahead of the upper tropospheric trough provides clouds with water vapor for deposition. The contrail cirrus cluster is transported eastward over the North Atlantic and remains for a long time in the ice supersaturated area.

Simulations of single contrail cirrus clusters were performed for two days each. We analyze the temporal evolution of contrail cirrus properties averaged over the whole contrail cirrus cluster, that is, over all grid boxes in which contrail cirrus exist. Microphysical properties are given as in-cloud values. Properties of natural cirrus are not displayed.

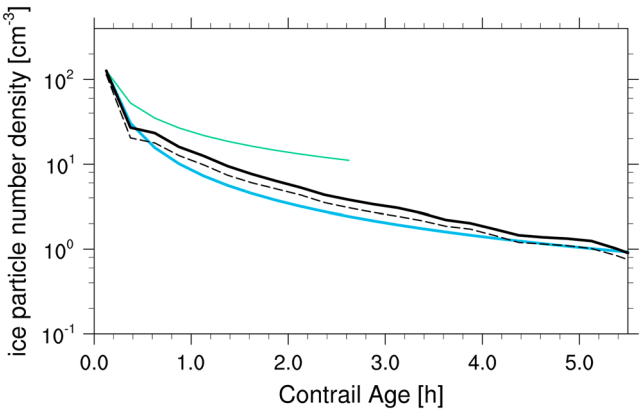

Figure 4. Temporal evolution of the mean in-cloud ice crystal number density (solid black line), averaged over the grid boxes where contrail cirrus exists, in comparison to the parameterization given by LES for a single contrail (blue line) [*Unterstrasser and Gierens*, 2010] and by a fit to dilution measurements (green line) [*Schumann et al.*, 1998]. For the calculation of the temporal evolution from the latter two parameterizations the initial ice crystal number concentration from the model simulation was prescribed. The dashed black line shows the mean ice crystal number density for a sensitivity run with a vertical diffusion coefficient twice as large as in the standard case.

3. Temporal Evolution of a Contrail Cirrus Cluster

3.1. Contrail Cirrus Volume

At the beginning of the contrail cirrus life cycle, the evolution of the contrail cirrus volume limits the water vapor available for deposition and therefore the deposition itself. After about 1.5 time steps (approximately 22 min) the contrail cross-sectional area is between 0.18 and 0.4 km^2 and lies therefore in the range derived from lidar measurements [*Freudenthaler et al.*, 1995]. The simulated in-cloud ice crystal number concentration averaged over the contrail cluster, which decreases as the contrail cirrus volume increases, is compared with a parameterization derived from detailed LES in Figure 4. The LES used for inferring the parameterization span the range of atmospheric variability in relative humidity and vertical wind shear that can be found in our GCM simulation. LES show that the ice particle concentration drops within about 5 h by about 2 orders of magnitude (Figure 4, blue line) [*Unterstrasser and Gierens*, 2010]. Depending on the prescribed relative humidity the decrease in ice crystal number concentration could vary by about 1 order of magnitude with differences in wind shear playing a minor role [*Unterstrasser and Gierens*, 2010]. Relative humidity at contrail formation and during the vortex regime has a strong impact since it determines the ice crystal number concentration after the vortex regime. The subsequent drop in ice crystal number concentration is approximately independent of relative humidity. As the dilution parameterization is independent of the initial ice crystal number, we prescribe our ice crystal number concentration at 7.5 min, well after the vortex phase. We compare our mean temporal evolution of dilution of the contrail cirrus cluster to the LES estimate for one single contrail.

Our simulated mean ice crystal concentration is in good agreement with the LES (Figure 4) showing a similar drop over 5 h. Differences in both simulations may be due to the constant cooling rate prescribed in the LES which determines the amount of water vapor available for deposition. The latter is in the GCM dependent on the synoptic situation and may vary significantly over time and space and has a strong impact on the sedimentation rate and the contrail volume. The decrease in ice crystal number concentrations simulated in this case study is slightly smaller than in the LES even when doubling the vertical diffusion coefficient, D_v, in the GCM parameterization. Considering only dilution due to mixing and turbulence as a growth process and neglecting growth due to sedimentation (Figure 4, green line) [*Schumann et al.*, 1998] the contrail cirrus volume grows much more slowly than simulated by the GCM. After about 1–2 h sedimentation becomes the dominant process for contrail cirrus volume growth in the GCM simulations and is significantly larger than in the dilution-only case. In the LES sedimentation seems to play a significant role even earlier judging from the fact that LES volume growth is much larger than when considering dilution only. In the first few time steps volume growth appears to be slightly too low in the GCM.

3.2. Increase in Ice Water Content Due to Deposition

The increase in ice water content is dependent on the contrail cirrus volume, in particular during the first few hours at flight level, the ice crystal number concentration and the water vapor available for deposition.

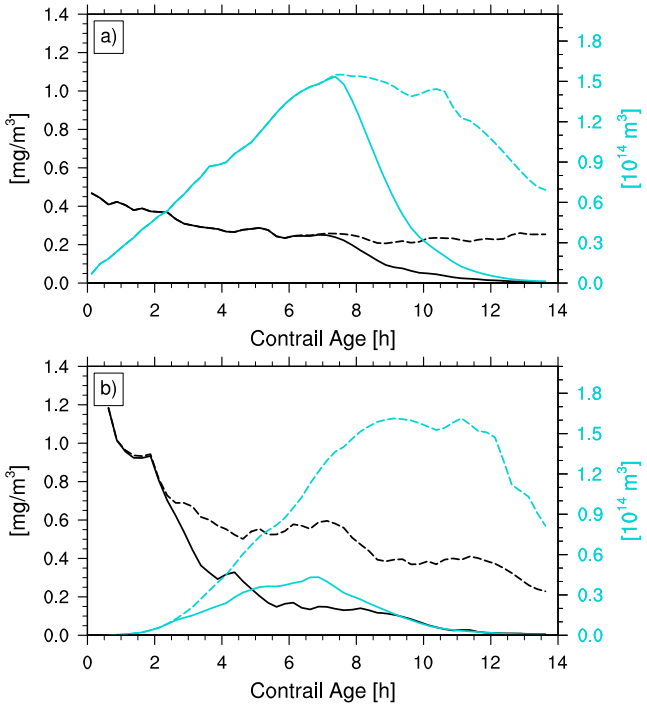

Figure 5. Temporal evolution of water vapor concentration available for deposition (black dashed line), ice water deposition per time step (black solid line), contrail cirrus volume (blue dashed line), and corrected volume for (a) deposition (blue solid line) in flight level and (b) one level below averaged over the grid boxes where contrail cirrus exists.

Due to turbulent diffusion and sedimentation the contrail cirrus volume increases (Figure 5, blue dashed line). At the beginning of the contrail cirrus lifetime, ice crystal number concentrations are so high that all the available water vapor within the contrail cirrus volume (black dashed line) can be deposited on the contrail cirrus ice crystals (black solid line). In our simulation, within a large-scale ice supersaturated area, this is the case at flight level for about the first 7 h (Figure 5a). In the level below (Figure 5b), where sedimenting contrail cirrus ice crystals dominate the ice crystal number concentration, this is only the case for the first 3 h. Later in the life cycle ice crystal number concentrations are so low that deposition is limited considerably. Ice supersaturation cannot be relaxed within one time step. Therefore, less water is deposited on the contrail cirrus ice crystals than is available. We calculate a corrected contrail volume for deposition (Figure 5, blue solid line) which corresponds to the part of the contrail cirrus volume in which ice supersaturation can be relaxed to saturation or in other words. At flight level the limitation of deposition at times of low ice crystal number concentrations has only a significant effect for very long lived contrails. In areas in which ice crystal number concentrations are controlled by sedimentation, water uptake is strongly limited by low ice crystal number concentrations. In those areas air within contrail cirrus remains ice supersaturated. The impact of the limitation of deposition rates on the ice water content is the integral of the difference between the water vapor available for deposition and water vapor deposited on ice crystals.

In Figure 6 we show the ratio of the corrected contrail cirrus volume, which indicates the part of the contrail cirrus volume in which ice supersaturation can be relaxed, and the total contrail cirrus volume. The ratio is strongly dependent on the ice particle number concentration (equation (5); Figure 6, colored asterisks). As long as the ice crystal number concentration lies above 1 cm^{-3}, the ratio of corrected and total contrail cirrus volume is equal to one which means that according to our approximation the water vapor concentration could be reduced to saturation. This agrees with observations [*Heymsfield et al.*, 1998; *Kaufmann et al.*, 2014] and LES [*Unterstrasser and Gierens*, 2010] that show ice saturation inside the contrail core because of the high ice particle number concentration. Dilution and sedimentation reduces ice crystal number concentration strongly, so that later on ice particle number density is too small (lower than 1 cm^{-3}) to accommodate all available water vapor. Therefore, the ratio is smaller than one and only a fraction of the available water vapor can be deposited and air remains supersaturated inside the contrail cirrus. Once ice crystal concentrations have dropped below

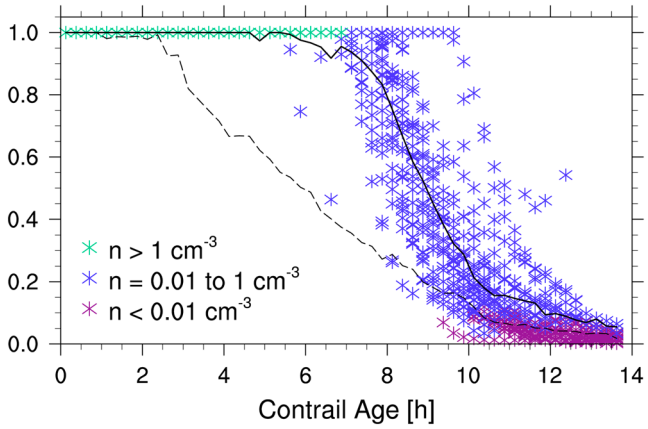

Figure 6. Mean temporal evolution of fraction of corrected contrail volume for deposition to total contrail volume per grid box at the pressure level of contrail formation (solid line) and one level below (280 hPa, dashed line). For the pressure level of contrail formation, contrail cirrus in-cloud ice particle number concentrations are color coded with purple indicating concentrations smaller than 0.01 cm^{-3}, blue for concentrations between 0.01 cm^{-3} and 1 cm^{-3} (blue) and green for concentrations greater than 1 cm^{-3}. Please note that starting at about 3 h after air traffic ice crystal number concentration drops in some grid boxes below 1 cm^{-3}. Associated blue crosses are hidden by the green ones.

0.01 cm^{-3}, less than 10% of available water vapor can be deposited and the contrail cirrus practically ceases to exist. In our case study this happens after around 12 h. In the level below the flight level ice particle number concentrations are much smaller from the start and the ratio of corrected and total contrail cirrus volume (Figure 6, dashed line) decreases much earlier leaving air ice supersaturated even in relatively young contrails.

3.3. Microphysical and Optical Properties of the Contrail Cirrus Cluster

Figure 7 shows the evolution of ambient humidity and contrail cirrus properties with time, both horizontally averaged over the contrail cirrus area, that is, over the grid boxes containing contrail cirrus. Water vapor available for deposition during one time step (Figure 7a) is largest in lower levels. It decreases slightly with time within the contrail cirrus volume.

Right after formation the ice crystal number concentration (Figure 7b) has its maximum (about 100 cm^{-3}) and mean ice particle sizes are on average 1 μm (Figure 7d), which compares well with measured sizes of newly formed contrails [*Schröder et al.*, 2000; *Febvre et al.*, 2009]. Ice crystal number concentrations decrease quickly to less than 1 cm^{-3} after about 5 h. Below the flight level ice crystal number concentrations are much lower. At about 300 hPa values are as low as 0.1 cm^{-3} within the contrail cirrus.

Ice water content (IWC, Figure 7c) increases quickly due to deposition of available water vapor, reaching at flight level maximum values between 1 and 6 h after formation. Afterward ice water content decreases again due to the fact that sedimentation reduces ice water content and ice crystal number concentration. The latter causes again a reduction in the deposition rate. This signature of increasing ice water content and a subsequent decrease with declining crystal number concentrations can be also found in LES [e.g., *Unterstrasser and Gierens*, 2010]. It is apparent that IWC is largest at the height of the contrail core or very slightly below due to the large ice crystal number density. At lower levels more water vapor is available for deposition (Figure 7a) but the ice crystal number concentration is too low to reduce ice supersaturation effectively. In the fall streaks ice particle number density is more than 1 order of magnitude smaller (Figure 7b), similar to what has been observed [*Heymsfield et al.*, 1998; *Schröder et al.*, 2000] and simulated using LES [*Unterstrasser and Gierens*, 2010; *Lewellen*, 2014]. Nevertheless, ice crystals grow faster in lower levels because more water vapor is on average available and reach on average up to 200 μm (Figure 7d) before sedimenting into subsaturated regions. The process rates show that in the level of contrail formation and above there is a continuing loss of ice crystals and water mass, whereas in levels below ice crystal number and mass grow by sedimentation, part of which, however, sublimate in subsaturated air which constitutes a sink in ice crystal number.

In our long-lived ice supersaturated area the lifetime of the contrail cirrus cluster is strongly controlled by sedimentation. Ice crystal number concentrations in our simulation are on average reduced by 3 orders

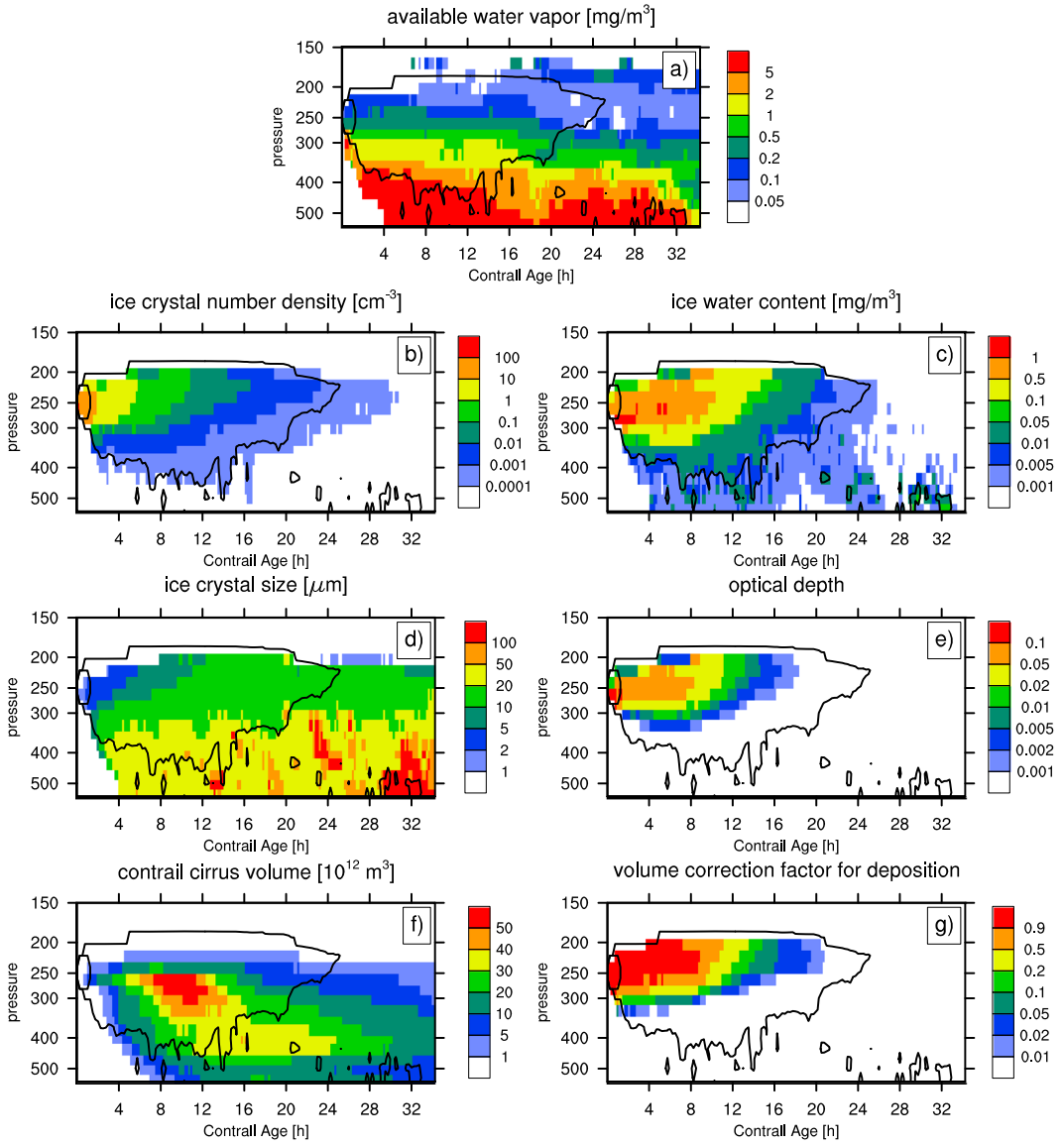

Figure 7. Temporal evolution of a contrail cirrus cluster and the available water vapor. (a) Mean water vapor concentration available for deposition per time step, (b) mean in-cloud ice crystal number density, (c) in-cloud ice water content, (d) ice crystal size, (e) optical depth, (f) total contrail cirrus volume, and (g) volume correction factor for deposition of a contrail cirrus cluster formed during 1 h from air traffic over the eastern part of the USA (34–44°N, 87–116°W, 260 hPa). Values are horizontal means or rather sums over the grid boxes where contrail cirrus exists. The black small oval indicates the air traffic height and time and the black solid line indicates the location and time for which contrails have on average an optical depth greater than 0.0001.

of magnitude after about 10 h due to dilution and sedimentation. Although water vapor continues to be available for deposition (Figure 7a), the decrease of ice crystal number concentration prevents a continuing water uptake and limits the lifetime of the contrail cirrus cluster. Only a few large contrail cirrus ice crystals remain. As described already in section 3.1, after about 7 h the contrail cirrus cluster has spread considerably (Figure 7f) and the ice crystal number concentration is so small that ice supersaturation can no longer be relaxed within a model time step at flight level (Figure 7g). This means that in such old contrail cirrus air is ice supersaturated. At lower levels, in which concentrations are controlled by sedimentation, this is the case nearly immediately. The contrail cirrus cluster displays on average an ice crystal number density and an ice crystal size of less than 1 cm^{-3} and 5 to 10 μm, after about 5–7 h and therefore resemble natural cirrus at flight level.

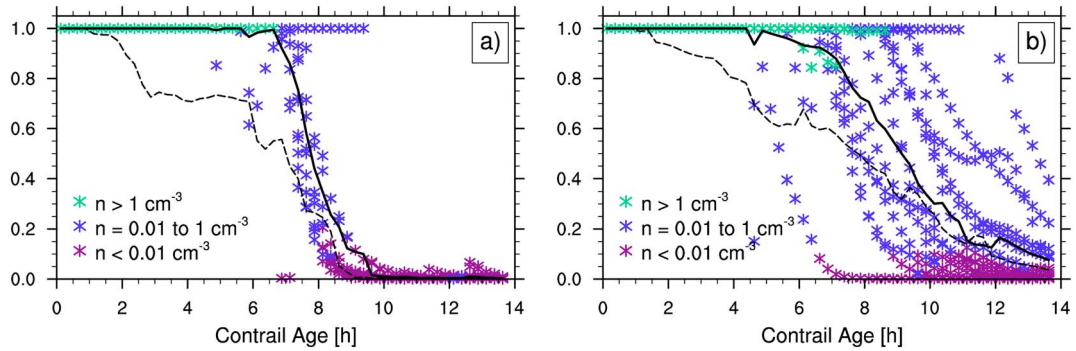

Figure 8. As Figure 6 but for (a) simulation 2 and (b) simulation 3. Please note that starting at about 4.5 h in simulation 2 and 3 h in simulation 3 after air traffic, ice crystal number concentration drops in some grid boxes below 1 cm^{-3}. Associated blue crosses are hidden by the green ones.

Optical depth, which is a measure for the radiative impact of the contrail cirrus cluster, is parameterized by the ice crystal number concentration and the IWC [*Lohmann and Kärcher*, 2002; *Roeckner et al.*, 2003]. After formation optical depth (Figure 7e) is largest because of the large number of small ice crystals. Later on, when ice crystal numbers decrease, ice water content increases due to deposition causing a sustained maximum in optical depth. With declining ice water content, optical depth declines as well. After 7 h average contrail cirrus optical depth at flight level is still 0.05, a threshold value for detectability from satellites [*Kärcher et al.*, 2009]. After about 9 h the contrail cirrus cluster is on average too optically thin to be visible (optical depth <0.02).

The contrail cirrus cluster simulated here evolved in a geographically and temporally extended ice supersaturated region. Nevertheless, the maxima of simulated contrail cirrus ice water content averaged over the whole contrail cirrus cluster (about 2 mg m^{-3}) and optical depth (about 0.1) lay in the lower range of satellite and in situ measurement [*Iwabuchi et al.*, 2012; *Minnis et al.*, 2013; *Bedka et al.*, 2013; *Schröder et al.*, 2000; *Voigt et al.*, 2011]. As we simulate the contrail cirrus cluster in January conditions, this could explain the lower values. The mean ice particle size of the 3–4 h old contrail cirrus cluster fits well with satellite measurements of line shaped contrails [*Minnis et al.*, 2013; *Bedka et al.*, 2013] which have on average ice crystal sizes of 14–22 µm.

3.4. Dependence on the Synoptic Situation

In order to study whether our main conclusions from the above simulation hold also in different synoptic settings we analyze two more simulations. We choose situations, in which contrail cirrus are particularly long lived and in which microphysical processes are important for the evolution of the contrail cirrus cluster. Long-lasting ice supersaturated areas are infrequent but of particular importance for contrail cirrus radiative forcing [*Burkhardt and Kärcher*, 2009]. Contrail cirrus form over the same region and season, in January (see section 2.3). One of the synoptic cases, simulation 2, is a long lasting but spatially very limited ice supersaturated area. The contrail cirrus cluster acquires a very high optical depth in this situation. The other case, simulation 3, is a large scale and long-lasting ice supersaturated area with a limited amount of water vapor available for deposition. The contrail cirrus developing in this system does not acquire as much ice water as the case described above and therefore the optical depth of the contrail cirrus cluster is smaller.

We find that both contrail cirrus cluster lifetimes are limited by the steady decrease in ice crystal number concentrations. The clusters are still situated in ice supersaturated areas and water vapor is still available for deposition but water vapor deposition on ice crystals is limited due to the low ice crystal number concentrations. Figure 8 shows the mean temporal evolution of the fraction of available water vapor that can be deposited on the contrail cirrus ice crystals at the pressure level of contrail formation (260 hPa). As for the contrail cirrus cluster discussed above for the first few hours all the available water vapor can be deposited on the contrail cirrus ice crystals with a sudden drop off at about 7 h for both cases. The drop off is more sudden in simulation 2 since the contrail cirrus cluster is smaller and therefore the background atmospheric state is more or less constant over the whole contrail cirrus cluster. Even though the development of the contrail cirrus clusters are quite different, the timing of the limitation of deposition due to low ice crystal number concentrations is surprisingly similar. This is particularly surprising since the variability within one contrail cirrus cluster can be extremely large. In simulation 3 different parts of the contrail cirrus cluster evolve very differently leading to a large variability in the timing of the limitation of deposition due to low crystal numbers.

Table 1. Duration in Hours Until Contrail Cirrus Cluster Reaches Listed Microphysical Properties at Flight Level

Experiment	$\Delta t/\tau^a < 1$	$n \leq 1\text{cm}^{-3}$	$r \geq 5\mu\text{m}$	$r \geq 10\mu\text{m}$
1	7	5	3.5	7
2	6.5	5.5	2.5	5
3	7	6–8	3.5	7

[a] See section 2.2.

Contrail cirrus evolve and eventually resemble natural cirrus in terms of ice crystal number concentrations ($n < 1\text{cm}^{-3}$) and crystal radii ($r > 5 - 10\mu\text{m}$). This happens slightly earlier, after about 5 to 5.5 h, in simulation 2 later, after about 6 to 8 h, in simulation 3 compared to the first idealized study discussed in the sections above. Table 1 summarizes the timing for all three simulations.

4. Conclusion and Outlook

In this paper we present a microphysical extension of the contrail cirrus parameterization of *Burkhardt and Kärcher* [2009] in the climate model ECHAM5. We use the microphysics scheme of *Lohmann et al.* [2008] and adapt it for the ice cloud regime to make it consistent with a fractional cloud cover scheme. The microphysical two-moment scheme is then introduced in the contrail cirrus scheme and the representation of contrail microphysical processes, in particular deposition, is improved. The temporal development of a contrail cirrus cluster has been studied. The early development of the contrail volume or ice crystal number concentration has been compared to LES. The development in a long-lived and large scale ice supersaturated area is studied. Overall we find that the microphysical extension described here had a significant impact on the life cycle and the microphysical and optical properties of the contrail cirrus cluster.

We reintroduced a fractional cloud cover scheme for ice clouds and parameterized homogenous nucleation events [*Kärcher and Lohmann*, 2002], assuming that in a new cloud area the homogeneous freezing level was reached. The representation of ice clouds was evaluated using in situ measurement data and a satellite simulator and found to be successful regarding ice cloud cover and IWC. Ice crystal number concentrations display a slight bias toward larger values relative to observations [*Jensen et al.*, 2013] in an area strongly influenced by convection. This is possibly a result of uncertainty due to the impact of convection and neglecting the effect of heterogenous nucleation. Ice supersaturation frequency was parameterized following *Burkhardt et al.* [2008] and compared to satellite observations of *Lamquin et al.* [2012]. It was found to be well captured except for an upward shift of large ice supersaturation frequency in the extratropical upper troposphere consistent with a too high tropopause.

Microphysical processes in the contrail cirrus scheme were parameterized as in the natural ice cloud scheme as far as possible. A parameterization has been added that describe the evolution of the contrail cirrus volume due to turbulent diffusion. The simulated decrease in ice crystal number concentration was shown to agree well with LES estimates. The decrease was slightly lower than suggested by the LES but significantly larger than when taking only dilution into account. At the beginning of the contrail life cycle, ice crystal number concentrations are so high that all the water vapor available for deposition is quickly deposited on the ice crystals. Secondary nucleation is not allowed inside contrail cirrus so that low ice crystal number concentrations can be found after a few hours in the contrail core area or early on in areas that are dominated by sedimentation. In those areas in-cloud ice supersaturation cannot be effectively reduced within a model time step and deposition must be estimated from the diffusional growth time scale.

We simulate a single contrail cirrus cluster that is initiated from air traffic over the eastern USA and subsequently drifts eastward over the Atlantic. The contrails are formed within 1 h, with air traffic being switched off afterward, so that the temporal development of the contrail cirrus cluster could be studied. The synoptic situation, in which the contrails are formed and develop, is characterized by a long-lived and large scale ice supersaturated area. This synoptic situation is ideally suited to studying the microphysical process rates and their effects during different stages of the contrail cirrus life cycle. Furthermore, those long-lived contrail cirrus clusters contribute strongly to the global contrail cirrus radiative forcing [*Burkhardt and Kärcher*, 2009]. The lifetime of the contrail cirrus cluster is in long-lived ice supersaturated areas not limited by the lifetime of the ice supersaturated area or the residence time of the contrail cirrus in it but by the microphysical processes

within the contrail cirrus. In those situations sedimentation is the most important process contributing to ice crystal loss. The simulated contrail cirrus cluster displays typical signatures as found in LES studies, such as the early increase in optical depth due to water vapor deposition despite a steady decrease in ice crystal number concentrations. After a few hours optical depth decreases due to low ice crystal number concentrations that start to limit water vapor deposition on ice crystals. This decrease in ice crystal number concentration and IWC eventually limits the lifetime of the contrail cirrus, a process that could not have been captured using a microphysical one-moment scheme.

In the contrail cirrus core area the ice crystal number concentration limits deposition after about 7 h and air within the contrail cirrus volume remains ice supersaturated. In areas below the contrail that are dominated by sedimentation, ice crystals are not able to relax ice supersaturation to saturation effectively after only a couple of hours and ice supersaturation occurs regularly.

At the beginning of the contrail life cycle microphysical properties of contrails are very distinct from those of natural cirrus, with ice crystal number concentrations of 10–100 cm^{-3} and ice crystal sizes of 1 μm as compared to less than 1 cm^{-3} and more than 5–10 μm for natural cirrus. In our case studies a contrail cirrus cluster has on average the latter properties after about 5–7 h and therefore resembles natural cirrus.

The improvements of the contrail cirrus parameterization introduced in this paper are aimed at reducing the uncertainty in contrail cirrus climate forcing estimates. An important step toward this goal is to improve the parameterization of physical processes governing the life cycle of contrail cirrus clouds in models [*Burkhardt et al.*, 2010]. The evaluation of the parameterization is hampered by the sparsity of appropriate data sets. Therefore, it is crucial to improve our understanding of the processes controlling the contrail cirrus evolution and compare GCM simulations with simulations and process understanding generated by LES. We believe that this is an important step toward improving the credibility of contrail cirrus simulations in climate models. Furthermore, a continued effort improving the representation of upper tropospheric humidity, natural clouds, and nucleation events in natural cirrus is important for reducing the uncertainty of contrail cirrus properties and radiative forcing.

In a following paper we will study the impact of the microphysical extension on contrail cirrus properties and the associated radiative forcing of contrail cirrus when considering global air traffic. We will also use this model setup for studying the impact of a reduction of initial ice crystal concentration as expected when using alternative fuels. We expect that the reduction of the initial ice crystal number has a significant impact on contrail cirrus cover, properties, and radiative forcing.

Appendix A: Contrail Cirrus Volume

Particular care has been taken to capture the increase in contrail cirrus volume due to ice crystal sedimentation and turbulent diffusion in the presence of wind shear. The contrail cirrus volume growth due to turbulent diffusion ($\left(\frac{\partial V}{\partial t}\right)_{\mathrm{dif}}$, equation (2)) is parameterized following *Dürbeck and Gerz* [1996]. Instead of calculating the growth of one particular contrail we calculate the mean growth of a number of contrails of a specified age. Due to the low temporal resolution of the climate model, we can set the horizontal and skewed diffusional coefficient to zero, because with increasing time they have a diminishing influence on the growth of the contrail cirrus cross section, A. The growth of A with time, t, is just dependent on wind shear, s, and vertical diffusion in the following way:

$$A(t) = 2\pi \left[\frac{1}{3}s^2 D_v^2 t^4 + \frac{2}{3}s^2 D_v \sigma_{v,0}^2 t^3 + 2D_v \sigma_{h,0}^2 t + \sigma_{v,0}^2 \sigma_{h,0}^2\right]^{1/2}. \tag{A1}$$

We initialize the initial horizontal and vertical plume standard deviation, $\sigma_{h,0}$ and $\sigma_{v,0}$, assuming that the contrail cirrus height and width at the time step of contrail initialization (7.5 min) correspond to three times the respective standard deviation. We use a typical vertical diffusion coefficient, D_v, for the tropopause region of 0.15 m^2/s [*Dürbeck and Gerz*, 1996]. We apply equation (A1) to the mean cross section of contrail cirrus of a particular age in each grid box and calculate the growth of the cross section and volume for all individual contrail cirrus age classes. This calculation requires distinguishing between the volume and length of contrail cirrus of different age classes (section 2.2). Figure A1a shows the relative growth of the contrail cross section for different values of shear. The higher the shear the faster the area cross section increase in the beginning. After about 150 min there is no difference between the shear cases since for larger shear the cross-sectional

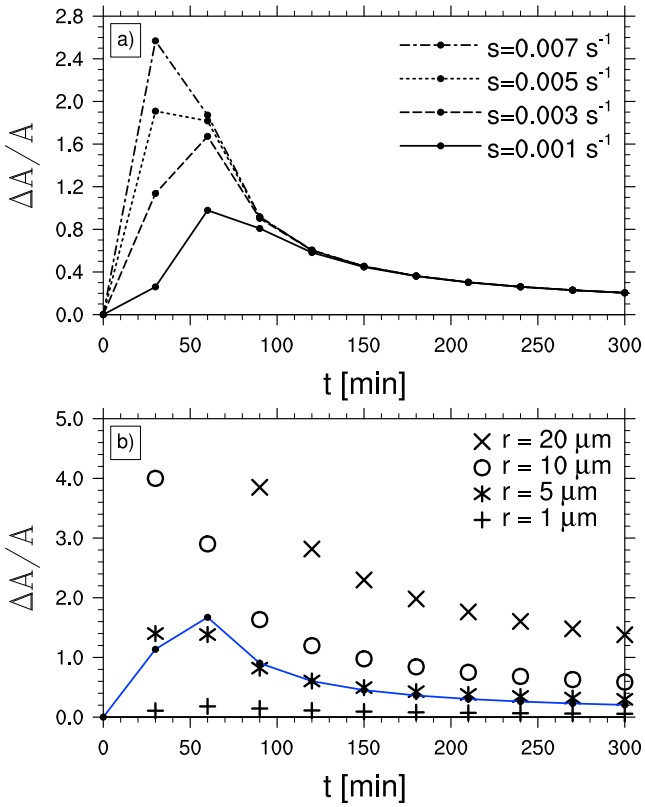

Figure A1. Temporal evolution of relative increase of contrail area cross section (a) by turbulent diffusion for various values of shear (s^{-1}) and (b) by sedimentation for different ice particle sizes (µm) within one time step (30 min). (For comparison, in Figure A1b the blue line shows the increase by turbulent diffusion with shear = 0.003 s^{-1}. The cross-sectional growth due to sedimentation is calculated each time step using A as starting point when assuming only growth by turbulent diffusion with a shear of 0.003 s^{-1}.)

increase and the cross section itself is larger than for low-shear cases. The relative increase is only dependent on the time step length, because for large values of t, the function $\Delta A/A$ is approximately identical to $2\Delta t/t$.

Early in the contrail lifetime the growth of A is dominated by diffusional growth, whereas later on, when contrail ice crystals have grown due to deposition of water vapor on the ice crystals, volume growth due to sedimentation ($\left(\frac{\partial V}{\partial t}\right)_{sed}$, equation (2)) is getting more important (Figure A1b). At this point the growth of the contrail cross-sectional area is determined by the interplay of wind shear and sedimentation. We estimate the increase in the height of the contrail using the fall velocity of the sedimenting ice crystals, assuming ice crystals with specified mean size, from the model's microphysics scheme and calculating the vertical displacement of the sedimenting ice crystals within a time step. The increase in contrail volume in Figure A1b is calculated from this contrail height increase and an estimate of the contrail width using a simplified version of the parameterization by *Dürbeck and Gerz* [1996] consistent to equation (A1):

$$\sigma_h^2 = \frac{2}{3}s^2 D_v t^2 + s^2\sigma_{v,0}^2 t^2 + \sigma_{h,0}^2. \quad \text{(A2)}$$

In the GCM simulations the contrail cirrus width is calculated from the horizontally spread contrail cirrus cover, which is controlled by the vertical wind shear as in the parameterization of *Burkhardt and Kärcher* [2009].

Acknowledgments
The authors thank Bernd Kärcher and Simon Unterstrasser for stimulating discussions and helpful comments on the manuscript, Andreas Bier for support with the simulations, Nicola Lamquin for providing observational data on ice supersaturation, Christine Nam and Johannes Quaas for providing the COSP simulator code, and three anonymous reviewers for their helpful comments and suggestions. The presented data can be obtained from the first author upon request (lisa.bock@dlr.de). The research was supported by the Bundesministerium für Wirtschaft und Technologie (BMWi) as a result of a decision of the Deutsche Bundestag within the project ATMOS-FAIR (20Y0904D). The model simulations were performed at the German Climate Computing Centre (DKRZ) through support from the Bundesministerium für Bildung und Forschung (BMBF).

References

Atlas, D., Z. Wang, and D. P. Duda (2006), Contrails to cirrus-morphology, microphysics, and radiative properties, *J. Appl. Meteorol. Climatol.*, *45*(1), 5–19.

Bedka, S., P. Minnis, D. Duda, T. Chee, and R. Palikonda (2013), Properties of linear contrails in the Northern Hemisphere derived from 2006 Aqua MODIS observations, *Geophys. Res. Lett.*, *40*, 772–777, doi:10.1029/2012GL054363.

Bodas-Salcedo, A., et al. (2011), COSP: Satellite simulation software for model assessment, *Bull. Am. Meteorol. Soc.*, *92*(8), 1023–1043.

Boucher, O., et al. (2013), Clouds and aerosols, in *Climate Change 2013: The Physical Science Basis. Contribution of Working Group I to the Fifth Assessment Report of the Intergovernmental Panel on Climate Change*, vol. 7, edited by T. Stocker et al., pp. 571–658, Cambridge Univ. Press, Cambridge, U. K., and New York.

Burkhardt, U., and B. Kärcher (2009), Process-based simulation of contrail cirrus in a global climate model, *J. Geophys. Res.*, *114*, D16201, doi:10.1029/2008JD011491.

Burkhardt, U., and B. Kärcher (2011), Global radiative forcing from contrail cirrus, *Nat. Clim. Change*, *1*, 54–58.

Burkhardt, U., B. Kärcher, M. Ponater, K. Gierens, and A. Gettelman (2008), Contrail cirrus supporting areas in model and observations, *Geophys. Res. Lett.*, *35*, L16808, doi:10.1029/2008GL034056.

Burkhardt, U., B. Kärcher, and U. Schumann (2010), Global modeling of the contrail and contrail cirrus climate impact, *Bull. Am. Meteorol. Soc.*, *91*(4), 479–484.

Chen, C.-C., A. Gettelman, C. Craig, P. Minnis, and D. Duda (2012), Global contrail coverage simulated by CAM5 with the inventory of 2006 global aircraft emissions, *J. Adv. Model. Earth Syst.*, *4*, M04003, doi:10.1029/2011MS000105.

Chepfer, H., D. Bony, D. Winker, G. Cesana, J. Dufresne, P. Minnis, C. Stubenrauch, and S. Zeng (2010), The GCM-Oriented CALIPSO Cloud Product (CALIPSO-GOCCP), *J. Geophys. Res.*, *115*, D00H16, doi:10.1029/2009JD012251.

Dürbeck, T., and T. Gerz (1996), Dispersion of aircraft exhausts in the free atmosphere, *J. Geophys. Res.*, *101*(D20), 26,007–26,016.

Eyers, C., P. Norman, J. Middel, M. Plohr, S. Michot, K. Atkinson, and R. Christou (2004), AERO2K global aviation emissions inventories for 2002 and 2025, *Tech. Rep., QINETIC/04/01113*, QinetiQ, Farnborough, U. K.

Febvre, G., J. Gayet, A. Minikin, H. Schlager, V. Shcherbakov, O. Jourdan, R. Busen, M. Fiebig, B. Kärcher, and U. Schumann (2009), On optical and microphysical characteristics of contrails and cirrus, *J. Geophys. Res.*, *114*, D02204, doi:10.1029/2008JD010184.

Freudenthaler, V., F. Homburg, and H. Jäger (1995), Contrail observations by ground-based scanning lidar: Cross-sectional growth, *Geophys. Res. Lett.*, *22*, 3501–3504.

Gehlot, S., and J. Quaas (2012), Convection-climate feedbacks in the ECHAM5 general circulation model: Evaluation of cirrus cloud life cycles with ISCCP satellite data from a Lagrangian trajectory perspective, *J. Clim.*, *25*(15), 5241–5259.

Heymsfield, A. J., R. P. Lawson, and G. W. Sachse (1998), Growth of ice crystals in a precipitating contrail, *Geophys. Res. Lett.*, *25*(9), 1335–1338.

Hoyle, C. R., B. P. Luo, and T. Peter (2005), The origin of high ice crystal number densities in cirrus clouds, *J. Atmos. Sci.*, *62*(7), 2568–2579.

ICAO (2007), *Environmental Report 2007*, Environ. Unit of the Int. Civ. Aviat. Organiz., Montreal, Canada.

Iwabuchi, H., P. Yang, K. Liou, and P. Minnis (2012), Physical and optical properties of persistent contrails: Climatology and interpretation, *J. Geophys. Res.*, *117*, D06215, doi:10.1029/2011JD017020.

Jensen, E., R. Lawson, J. Bergman, L. Pfister, T. Bui, and C. Schmitt (2013), Physical processes controlling ice concentrations in synoptically forced, midlatitude cirrus, *J. Geophys. Res. Atmos.*, *118*, 5348–5360, doi:10.1002/jgrd.50421.

Jensen, E. J., A. S. Ackerman, D. E. Stevens, O. B. Toon, and P. Minnis (1998), Spreading and growth of contrails in a sheared environment, *J. Geophys. Res.*, *103*(D24), 31,557–31,567.

Jensen, E. J., et al. (2009), On the importance of small ice crystals in tropical anvil cirrus, *Atmos. Chem. Phys.*, *9*(15), 5519–5537.

Kärcher, B., and U. Burkhardt (2008), A cirrus cloud scheme for general circulation models, *Q. J. R. Meteorol. Soc.*, *134*(635), 1439–1461.

Kärcher, B., and U. Lohmann (2002), A parameterization of cirrus cloud formation: Homogeneous freezing of supercooled aerosols, *J. Geophys. Res.*, *107*(D2), 4010, doi:10.1029/2001JD000470.

Kärcher, B., and J. Ström (2003), The roles of dynamical variability and aerosols in cirrus cloud formation, *Atmos. Chem. Phys.*, *3*(3), 823–838.

Kärcher, B., and C. Voigt (2006), Formation of nitric acid/water ice particles in cirrus clouds, *Geophys. Res. Lett.*, *33*, L08806, doi:10.1029/2006GL025927.

Kärcher, B., J. Hendricks, and U. Lohmann (2006), Physically based parameterization of cirrus cloud formation for use in global atmospheric models, *J. Geophys. Res.*, *111*, D01205, doi:10.1029/2005JD006219.

Kärcher, B., U. Burkhardt, S. Unterstrasser, and P. Minnis (2009), Factors controlling contrail cirrus optical depth, *Atmos. Chem. Phys.*, *9*, 6229–6254.

Kärcher, B., U. Burkhardt, A. Bier, L. Bock, and I. J. Ford (2015), The microphysical pathway to contrail formation, *J. Geophys. Res. Atmos.*, *120*, 7893–7927, doi:10.1002/2015JD023491.

Kaufmann, S., C. Voigt, P. Jessberger, T. Jurkat, H. Schlager, A. Schwarzenboeck, M. Klingebiel, and T. Thornberry (2014), In situ measurements of ice saturation in young contrails, *Geophys. Res. Lett.*, *41*, 702–709, doi:10.1002/2013GL058276.

Korolev, A. V., and I. P. Mazin (2003), Supersaturation of water vapor in clouds, *J. Atmos. Sci.*, *60*(24), 2957–2974.

Kurz, C. (2007), Entwicklung und Anwendung eines gekoppelten Klima-Chemie-Modellsystems: Globale Spurengastransporte und chemische Umwandlungsprozesse, Doctoral thesis, Ludwigs-Maximilians-Universität München, München, Germany, DLR Forschungsbericht 2007–12. [Available at https://edoc.ub.uni-muenchen.de/4804/.]

Lamquin, N., C. Stubenrauch, K. Gierens, U. Burkhardt, and H. Smit (2012), A global climatology fo upper-tropospheric ice supersaturation occurence inferred from the Atmospheric Infrared Sounder calibrated by MOZAIC, *Atmos. Chem. Phys.*, *12*, 381–405.

Lee, D., D. Fahey, P. Forster, P. Newton, R. Wit, L. Lim, B. Owen, and R. Sausen (2009), Aviation and global climate change in the 21st century, *Atmos. Environ.*, *43*(22–23), 3520–3537.

Lewellen, D. C. (2014), Persistent contrails and contrail cirrus. Part II: Full lifetime behavior, *J. Atmos. Sci.*, *71*(12), 4420–4438.

Lohmann, U., and S. Ferrachat (2010), Impact of parametric uncertainties on the present-day climate and on the anthropogenic aerosol effect, *Atmos. Chem. Phys.*, *10*, 11,373–11,383.

Lohmann, U., and B. Kärcher (2002), First interactive simulations of cirrus clouds formed by homogeneous freezing in the ECHAM general circulation model, *J. Geophys. Res.*, *107*(D10), 4105, doi:10.1029/2001JD000767.

Lohmann, U., P. Spichtinger, S. Heidt, T. Peter, and H. Smit (2008), Cirrus clouds and ice supersaturation regions in a global climate model, *Environ. Res. Lett.*, *3*, 045022.

Meerkötter, R., U. Schumann, D. Doelling, P. Minnis, T. Nakajima, and Y. Tsushima (1999), Radiative forcing by contrails, *Ann. Geophys.*, *17*, 1080–1094.

Minnis, P., S. Bedka, D. Duda, K. Bedka, T. Chee, J. Ayers, R. Palikonda, D. Spangenberg, K. Khlopenkov, and R. Boeke (2013), Linear contrail and contrail cirrus properties determined from satellite data, *Geophys. Res. Lett.*, *40*, 3220–3226, doi:10.1002/grl.50569.

Nam, C., and J. Quaas (2012), Evaluation of clouds and precipitation in the ECHAM5 general circulation model using CALIPSO and CloudSat satellite data, *J. Clim.*, *25*(14), 4975–4992.

Paoli, R., and K. Shariff (2016), Contrail modeling and simulation, *Annu. Rev. Fluid Mech.*, *48*, 393–427.

Paoli, R., L. Nybelen, J. Picot, and D. Cariolle (2013), Effects of jet/vortex interaction on contrail formation in supersaturated conditions, *Phys. Fluids*, *25*(5), 053305.

Pruppacher, H., and J. Klett (1996), *Microphysics of Clouds and Precipitation*, Kluwer Acad., Dordrecht, Netherlands.

Roeckner, E., et al. (2003), The atmospheric general circulation model ECHAM5. Part 1: Model description, *Max-Planck-Inst. Rep. 349*, 127 pp., Max-Planck-Inst., Hamburg, Germany.
Schiller, C., M. Krämer, A. Afchine, N. Spelten, and N. Sitnikov (2008), Ice water content of Arctic, midlatitude, and tropical cirrus, *J. Geophys. Res.*, *113*, D24208, doi:10.1029/2008JD010342.
Schröder, F., B. Kärcher, C. Duroure, J. Ström, A. Petzold, J. Gayet, B. Strauss, P. Wendling, and S. Borrmann (2000), On the transition of contrails into cirrus clouds, *J. Atmos. Sci.*, *57*, 464–480.
Schumann, U. (1996), On conditions for contrail formation from aircraft exhausts, *Meteorol. Z.*, *5*, 4–23.
Schumann, U. (2002), Contrail cirrus, in *Cirrus*, edited by D. K. Lynch et al., pp. 231–255, Oxford Univ. Press, New York.
Schumann, U. (2012), A contrail cirrus prediction model, *Geosci. Model Dev.*, *5*(3), 543–580.
Schumann, U., H. Schlager, F. Arnold, R. Baumann, P. Haschberger, and O. Klemm (1998), Dilution of aircraft exhaust plumes at cruise altitudes, *Atmos. Environ.*, *32*(18), 3097–3103.
Stier, P., et al. (2005), The aerosol-climate model ECHAM5-HAM, *Atmos. Chem. Phys.*, *5*, 1125–1156.
Sundqvist, H. (1978), A parameterization scheme for non-convective condensation including prediction of cloud water content, *Q. J. R. Meteorol. Soc.*, *104*, 677–690.
Unterstrasser, S. (2014), Large-eddy simulation study of contrail microphysics and geometry during the vortex phase and consequences on contrail-to-cirrus transition, *J. Geophys. Res. Atmos.*, *119*, 7537–7555, doi:10.1002/2013JD021418.
Unterstrasser, S., and K. Gierens (2010), Numerical simulations of contrail-to-cirrus transition-part 1: An extensive parametric study, *Atmos. Chem. Phys.*, *10*(4), 2017–2036.
Voigt, C., U. Schumann, P. Jessberger, T. Jurkat, A. Petzold, J. Gayet, M. Krämer, T. Thornberry, and D. Fahey (2011), Extinction and optical depth of contrails, *Geophys. Res. Lett.*, *38*, L11806, doi:10.1029/2011GL047189.
Wang, Z., and K. Sassen (2002), Cirrus cloud microphysical property retrieval using lidar and radar measurements. Part II: Midlatitude cirrus microphysical and radiative properties, *Am. Meteorol. Soc.*, *59*, 2291–2302.